

# The Effective Removal of Methylene Blue Dye from Aqueous Solutions by NaAlg-g-Poly(acrylic acid-co-acryl amide)/Clinoptilolite Hydrogel Nanocomposite

Azam Rashidzadeh, Ali Olad\*, and Dariush Salari<sup>1</sup>

*Polymer Composite Research Laboratory, Department of Applied Chemistry, Faculty of Chemistry, University of Tabriz, Tabriz, Iran*

<sup>1</sup>*Petroleum Research Laboratory, Department of Applied Chemistry, Faculty of Chemistry, University of Tabriz, Tabriz, Iran*  
(Received October 14, 2013; Accepted October 11, 2014)

**Abstract:** A novel sodium alginate-g-poly(acrylic acid-co-acryl amide)/clinoptilolite hydrogel nanocomposite was prepared via free radical polymerization method, using N,N'-methylenebisacrylamide as a crosslinker and ammonium persulfate as an initiator. Grafting and component interactions were evidenced by Fourier transform infrared spectroscopic method. Adsorption properties of the both hydrogel samples in the aqueous solution of methylene blue (MB) dye were also investigated. Further investigations showed that methylene blue adsorption kinetic data followed pseudo-second-order kinetics. Also, adsorption equilibrium data were better fitted by a Freundlich isotherm. Finally the hydrogel nanocomposite designed in this work is distinguished by significantly higher adsorption capability, reusability, and stability making it an economical and successful adsorbent to remove MB dye from aqueous solutions.

**Keywords:** Nanocomposites, Hydrogel, Clinoptilolite, Poly(acrylic acid-co-acryl amide), Removal

## Introduction

Continuous releasing of dye stuffs and dye wastewater is a major concern due to their extremely harmful effects on the environment pollution and also people health. Textile, paper, plastics, leather, cosmetic, and paint industries are big consumers of dyes and thus effluents of these industries contain a wide variety of dyes which generate a considerable amount of toxic wastewater [1]. There are various forms of dyes including anionic dyes (direct, acid, and reactive), cationic (basic) dyes, and non-ionic (dispersed) dyes [2,3]. Methylene blue (MB) is the most commonly used cationic dye for dyeing cotton, wool, and silk. It is a severe eye and skin irritant and can cause nausea and stomach pain if swallowed [4,5]. Therefore, the treatment of effluent containing such dye because of its harmful impacts on human is of great interest.

The methods of dye removal from industrial wastewaters contain many processes such as biological treatment, coagulation, flotation, electrochemical techniques, adsorption, and oxidation [6,7]. Among these methods, the adsorption method is an effective and economical method for the removal of dyes from wastewater because this method can be used to remove different types of dye materials [8]. Adsorption method because of its low cost, high efficiency, ease of operation, and availability of different adsorbents is frequently used [9]. Different kinds of the adsorbents are generally used for dye removal. Different kinds of adsorbents are generally used for dye removal. Activated carbon [10], clays [11,12], natural zeolites [13], industrial byproducts and

wastes [14,15], natural polymers [16], and hydrogels [17,18] are common adsorbents used for removal of dyes.

Hydrogels are three-dimensional networks of hydrophilic polymer chains that can absorb large amounts of water, saline solutions, or other liquids up to several times of their dry weight [19]. By virtue of the unique three-dimensional network structure and various functional groups, hydrogels has become one of the new types of polymeric materials which have found extensive applications in various fields like water and wastewater treatment [20]. Besides that, inclusion of inorganic materials into hydrogels improves their swelling property and therefore adsorption capacity [21]. Among inorganic materials, natural zeolites like clinoptilolite due to their large surface area, valuable ion exchange capability, and low cost have gained significant interest for adsorption of dyes as adsorbent in wastewaters containing dyes and metals [22,23]. Besides that, the negative surface charge of zeolites makes them suitable for ion exchange process with cationic dyes [24]. Furthermore, the incorporation of these natural inorganic materials not only reduces production costs but also improves the swelling ability and mechanical and thermal stability of hydrogels [25]. The majority of hydrogels are made from synthetic hydrophilic polymers such as poly(acrylic acid) or its copolymer with poly(acrylamide) [26] while the demand for using natural hydrogels such as cellulose [27], starch [28], chitosan [29], and alginate [30] as adsorbents due to their biodegradability and low costs is continuously increasing. Alginate is a natural renewable and biodegradable polymer which has a high capacity to remove toxic pollutants like dyes from wastewater [31].

In the present work we report the synthesis of a novel

\*Corresponding author: a.olad@yahoo.com

hydrogel through graft copolymerization of acrylic acid (AA) and acrylamide (AAM) on sodium alginate in the presence of clinoptilolite. Also the adsorption capacity of MB using hydrogel nanocomposite was studied and the parameters influencing the adsorption capacity of the hydrogel like initial methylene blue dye solution concentration and amount of adsorbent were also investigated.

## Experimental

### Materials

Sodium alginate (NaAlg), acrylic acid (AA), acrylamide (AAM), N,N'-methylenebisacrylamide (MBA, as crosslinker), and ammonium persulfate (APS, as initiator) were purchased from Merck and were used without further purification. Methylene blue (MB) dye (Merck) was selected as cationic dye to study the adsorption capacity of prepared hydrogel nanocomposite. Table 1 shows the structure and characteristics of MB dye. Clinoptilolite (Clino) was supplied from Meianah mine in East Azerbaijan, Iran. The elemental composition of the raw clinoptilolite used in this work obtained by X-ray fluorescence (XRF) is given in Table 2. Other agents used were all analytical grade and all solutions were prepared with distilled water.

### Preparation of NaAlg-g-Poly (AA-co-AAM)/Clino Hydrogel Nanocomposite

A calculated amount of NaAlg powder was dissolved in distilled water and after dispersing certain amount of clinoptilolite (2-20 wt%) in above solution for 24 h, the solution was charged in a 250-ml four necked flask equipped with a mechanical stirrer, reflux condenser, a thermometer, and a nitrogen line. After being purged with nitrogen for 30 min to remove oxygen dissolved in the solution and heating to 60 °C in a water bath, the calculated amount of APS solution as initiator was added. After 15 min, the certain amount of AAM was added to the solution. Then mixture

solution of AA (partially neutralized by NaOH 6 mol/l solution, 70 % neutralization degree) and MBA as crosslinker (about 0.78 wt% of monomers) was charged into the flask drop wise. The water bath was heated slowly to 70 °C and kept for 4 h to complete polymerization. Finally, the resulting gel product was dried to constant weight at 70 °C and the dried gel product was ground and stored in dye place. The preparation procedure of NaAlg-g-poly(AA-co-AAM) hydrogels is similar to that of the NaAlg-g-poly(AA-co-AAM)/Clino hydrogel nanocomposite except without the addition of clinoptilolite. After formation of the hydrogel, the product was purified by immersing in distilled water for 4 days to remove the unreacted chemicals, during this time the water was changed once every 8 h. Then hydrogel product was also dried at 70 °C until constant weight and used for adsorption studies.

### Adsorption Studies

Adsorption experiments were done in batch mode technique. The hydrogel samples (200 mg) were added into MB dye solution (100 ml) with concentration of 25 mg/l. Then the concentration of residual dye in the solution was determined spectrophotometrically by measuring absorbance of dye solution at  $\lambda_{\max}$  of 665 nm for MB using the calibration curve. The adsorption capacity was calculated by the following formula:

$$Q_e = \frac{(C_i - C_e)V}{m} \quad (1)$$

where  $Q_e$  is the adsorption capacity or amount of MB dye adsorbed by hydrogel (mg/g),  $C_i$  is the initial MB dye concentration (mg/l),  $C_e$  is the equilibrium concentration of dye (mg/l),  $V$  is the volume of the dye solution (l), and  $m$  is the amount of hydrogel (g). Also, the removal efficiency of MB was calculated according to equation (2).

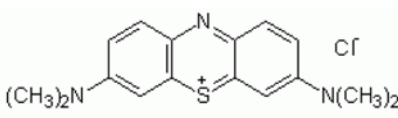
$$\text{Removal efficiency (R\%)} = \frac{C_i - C}{C_i} \times 100 \quad (2)$$

where  $C_i$  is the initial MB concentration,  $C$  is the concentration of unremoved MB after certain exposure time.

Also, the dependence of adsorption capacities on the contact time was investigated and the kinetics of adsorption was studied in detail. Furthermore, adsorption isotherms were obtained by agitating hydrogel samples in the dye solutions with concentrations ranging from 10 to 200 mg/l for a period of time equal to the respective equilibrium times.

Desorption studies were performed by contacting used adsorbents with HCl (0.1 M) solution and agitated for 24 h.

**Table 1.** Structure and characteristics of methylene blue dye

Structure	
Chemical formula	$C_{16}H_{18}ClN_3S$
Molar mass	319.85 g/mol
IUPAC name	3,7-bis(dimethylamino)phenothiazin-5-ium chloride

**Table 2.** Chemical composition of meianah clinoptilolite

Component (%)	SiO <sub>2</sub>	Al <sub>2</sub> O <sub>3</sub>	Fe <sub>2</sub> O <sub>3</sub>	CaO	MgO	Na <sub>2</sub> O	K <sub>2</sub> O	P <sub>2</sub> O <sub>5</sub>	MnO	TiO <sub>2</sub>	L.O.I
	65	12.03	1.5	2.3	0.72	1.8	3	0.01	0.1	0.03	13.51

Then the desorbed amount of MB was obtained spectrophotometrically. Desorption ratio was calculated using equation (3).

$$\text{Desorption ratio} = \frac{C}{C_0} \times 100 \quad (3)$$

where  $C$  is the amount of MB dye desorbed to the elution medium,  $C_0$  is the amount of MB dye adsorbed on the adsorbent. To determine the reusability of the nanocomposite, consecutive adsorption-desorption cycle was repeated for five times with the same hydrogel sample.

## Results and Discussion

### FT-IR Spectra

FT-IR is a good technique for investigating intermolecular interactions of certain functional groups and formation of hydrogen bonds in a random copolymer hydrogel such as poly(acrylic acid-co-acrylamide) will influence these molecular interactions. The FT-IR spectra of the NaAlg-g-p(AA-co-AAm)/Clin (20 wt% clinoptilolite), NaAlg-g-p(AA-co-AAm), and MB adsorbed NaAlg-g-p(AA-co-AAm)/Clin are shown in Figure 1(a)-(c), respectively. In Figure 1(a) and 1(b) the characteristic absorption bands of NaAlg around 1650  $\text{cm}^{-1}$  and 1450  $\text{cm}^{-1}$  due to carboxylate stretching vibrations can be seen. The broad band at 3000-3500  $\text{cm}^{-1}$  is due to the stretching absorption of the hydroxyl groups of the polysaccharide. The bands between 1000-1200  $\text{cm}^{-1}$  are attributed to the O-C-O stretching of ether groups and -C-O stretching of alcoholic groups [32]. The absorption bands of O-C-O stretching of ether groups and -C-O stretching of alcoholic groups in NaAlg disappeared in the IR spectrum of hydrogel samples, suggesting the grafting reaction of AA and AAm on NaAlg [33]. Also, the strong broad band at 1039  $\text{cm}^{-1}$

in Figure 1(a) corresponding to C-O stretching of alcoholic groups of alginate disappears in Figure 1(b) probably due to the covalent interactions between the components facilitated by crosslinking agent. Therefore in the case of NaAlg-g-p(AA-co-AAm)/Clin hydrogel nanocomposite some alcoholic groups from alginate may still be unreacted and free [34]. In Figure 1(a) and 1(b), the bands at 1683 and 1709  $\text{cm}^{-1}$  (respectively), are related to the overlapped stretching vibration of the carbonyl group of both AA and AM as well as the NH bending [35]. Also, the observed intense bands at 3426 (1a) and 3397 (1b)  $\text{cm}^{-1}$  are due to the overlapping absorption bands of O-H (from AA and hydrogen bonding) and stretching vibrations of N-H groups. Furthermore the absorption bands observed in the 1150-1350  $\text{cm}^{-1}$  region are related to the overlapping of the stretching C-N and C-O coupled with the bending of O-H groups [36]. The bands appear at 2945 and 2925  $\text{cm}^{-1}$  in Figure 1(a) and 1(b), corresponding respectively to the combined stretching of  $\text{CH}_2$  groups in both AA and AM in portions of the hydrogel structure. Also we can see two bands at 1408 and 1410  $\text{cm}^{-1}$  related to COO- group in polyacrylate and the peaks at 1454 (1a) and 1453 (1b) represent the C-N bonding, respectively. The peak at 1113  $\text{cm}^{-1}$  in Figure 1(a) due to the existence of Si-O group of clinoptilolite is not observed in Figure 1(b), which indicates the incorporation of the clinoptilolite into the hydrogel. It is worth to mention that in Figure 1(a), the peaks of carbonyl from 1709 (in Figure 1(b)) shifted to around 1683  $\text{cm}^{-1}$ . It may be because of the formation of hydrogen bonding between COOH of the hydrogel and hydroxyl groups of Al-OH and Si-OH in clinoptilolite [37].

The infrared spectrum of Na-Alg-g-p(AA-co-AAm)/Clin hydrogel nanocomposite after adsorption of MB dye is shown in Figure 1(c). The functional groups such as  $\text{NH}_2$ , -COOH, -OH in hydrogel may have interaction with MB dye. Studies have shown that carboxyl and hydroxyl groups are the most important groups responsible for the adsorption of MB. The shift of these bands in the case of MB adsorbed hydrogel nanocomposite indicated the interaction of these functional groups with  $=\text{N}(\text{CH}_3)_2^+$  group of MB molecules which results in the adsorption of MB dye by in the prepared hydrogel. FTIR spectrum indicated that large numbers of hydroxyl and carboxyl groups on the surface of hydrogel as well as negatively charged clinoptilolite zeolite may be the major adsorption sites for cationic dye of MB.

### XRD Patterns

Analysis of X-ray diffraction (XRD) patterns was used to investigate the structure and crystallinity of NaAlg-g-p(AA-co-AAm) hydrogel and NaAlg-g-p(AA-co-AAm)/Clin hydrogel nanocomposite. An X-ray diffractometer (XRD) D500 Siemens (Germany) was used to study the crystallinity of materials. Figure 2 shows the XRD patterns of pristine clinoptilolite NaAlg-g-p(AA-co-AAm) hydrogel, and NaAlg-g-p(AA-co-AAm)/Clin hydrogel nanocomposite.

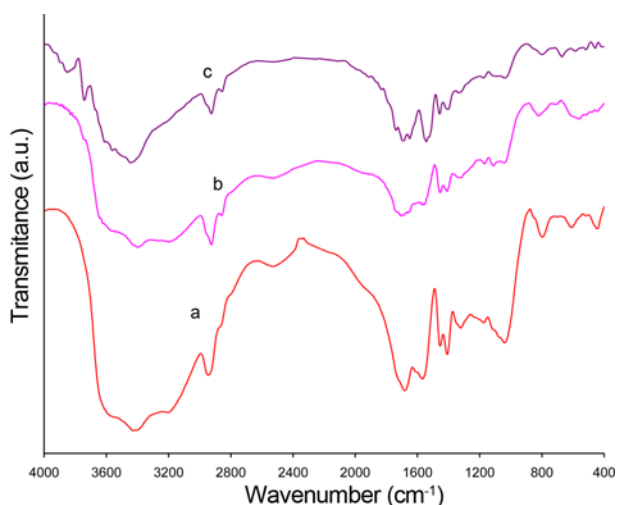


**Figure 1.** The FT-IR spectra of the NaAlg-g-p(AA-co-AAm)/Clin (a), NaAlg-g-p(AA-co-AAm) (b), and MB adsorbed NaAlg-g-p(AA-co-AAm)/Clin (c).

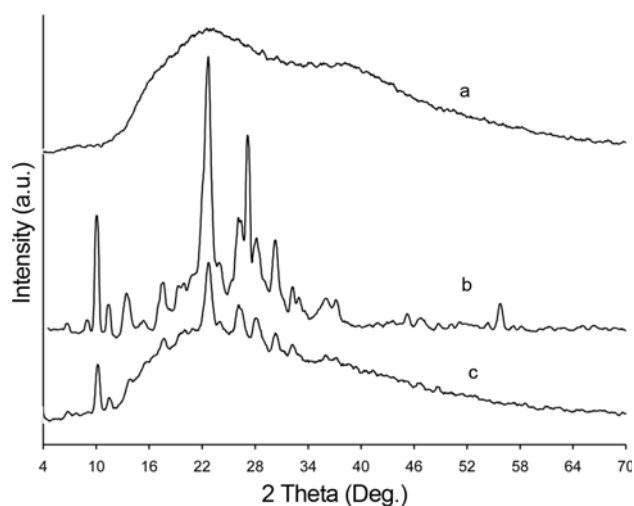


**Figure 2.** The XRD patterns of NaAlg-g-p(AA-co-AAm) hydrogel (a), pristine Clin (b), and NaAlg-g-p(AA-co-AAm)/Clin hydrogel nanocomposite (c).

As shown in Figure 2, the diffraction peaks appeared at  $2\theta=9.85^\circ$  and  $22.4^\circ$  are due to the Miller indexes of 020 and 004, respectively, in clinoptilolite [38] which indicates that the crystalline structure of clinoptilolite. The XRD patterns of NaAlg-g-p(AA-co-AAm) hydrogel has weak broad peaks at  $2\theta=22^\circ$  and  $2\theta=38^\circ$  because of its amorphous structure with low crystallinity. Figure 2 shows the X-ray diffraction patterns of NaAlg-g-p(AA-co-AAm)/Clin hydrogel nanocomposite, too. As seen before, NaAlg-g-p(AA-co-AAm) hydrogel has a typical noncrystalline (amorphous) pattern, while the NaAlg-g-p(AA-co-AAm)/Clin hydrogel nanocomposite had the typical crystallite reflections associated with the zeolite component. The presence of the peaks related to the clinoptilolite in the XRD pattern recorded for NaAlg-g-p(AA-co-AAm)/Clin hydrogel nanocomposite, confirms the presence of clinoptilolite in the nanocomposite composition. Also, deposition of NaAlg-g-p(AA-co-AAm) hydrogel on the outer and inner surfaces of clinoptilolite lattice channels, improves the alignment of NaAlg-g-p(AA-co-AAm) hydrogel chains and as a result, the intensity of the peaks related to the NaAlg-g-p(AA-co-AAm) hydrogel in the nanocomposite increases.

### Investigation of Surface Morphology

The surface morphology of hydrogel nanocomposite was studied using scanning electron microscopy (SEM). The SEM image of hydrogel nanocomposite is shown in Figure 3, which displays the porous structure of hydrogel nanocomposite. As it can be seen, SEM micrograph of hydrogel nanocomposite is composed of pores in the range of ten microns diameter with interconnected rooms inside which makes it more attractive for the adsorption of dye molecules.

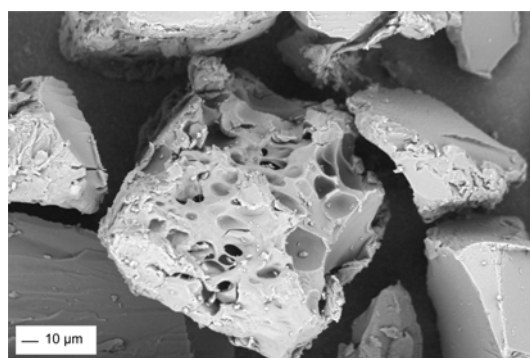


**Figure 3.** SEM micrographs of hydrogel nanocomposite.

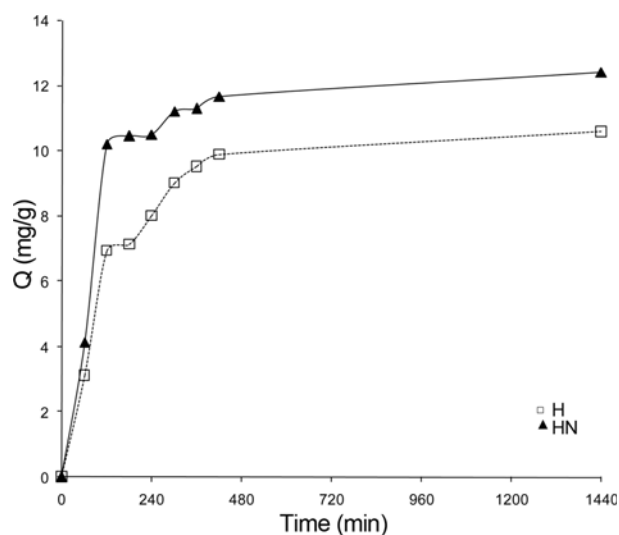


**Figure 4.** The effect of contact time on the adsorption capacity of MB.

### Adsorption Studies

#### Adsorption Kinetics

Rapid adsorption and high capacity are the main important factors in the treatment of wastewater containing dye molecules. To investigate this property, the H and HN hydrogel samples were left in MB dye solution (25 mg/l) and their capacities were determined at various time intervals. Change of adsorption capacities hydrogel samples with time was shown in Figure 4. It was clearly seen that with increasing treatment time the removal capacities of both hydrogels increased rapidly during 4 h and then slowed down and reached almost equilibrium value in 24 h. The efficient adsorption process is due to the functional groups, such as  $-NH_2$ ,  $-COOH$ ,  $-OH$ , etc., and unique network structure of the hydrogel. In order to understand the controlling mechanism of the adsorption process, several kinetic models were used to test the experimental data. In this work, the adsorption data were analyzed using two kinetic models, the pseudo-first-order [39] and pseudo-second-order [40] kinetic models, equation

(4) and equation (5), respectively.

$$\log(Q_e - Q_t) = \log Q_e - \frac{k_1}{2.303} t \tag{4}$$

$$\frac{t}{Q_t} = \frac{1}{k_2 Q_e^2} + \frac{1}{Q_e} t \tag{5}$$

where  $Q_e$  (mg/g) is the MB dye concentration at equilibrium,  $Q_t$  (mg/g) is MB dye molecule concentration at time  $t$ ,  $k_1$  ( $\text{min}^{-1}$ ) is the rate constant of the pseudo-first-order sorption, and  $k_2$  ( $\text{g} \cdot \text{mg}^{-1} \cdot \text{min}^{-1}$ ) is the pseudo-second-order sorption

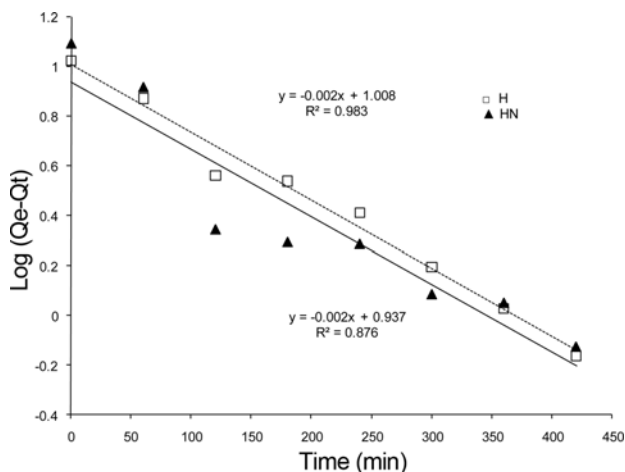


**Figure 5.** Pseudo first-order model for MB adsorption using hydrogel samples.

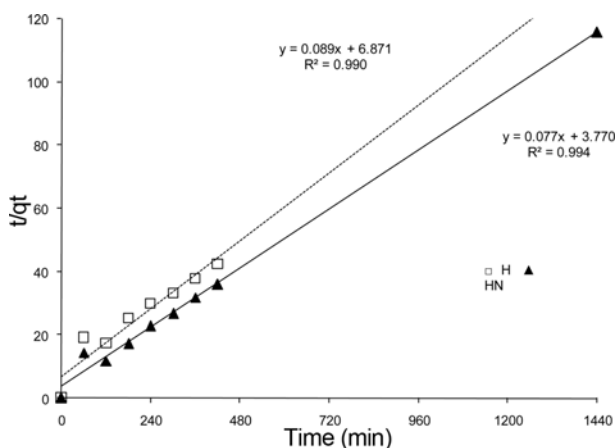


**Figure 6.** Pseudo second-order model for MB adsorption using hydrogel samples.

rate constant.

The linear plot of  $\log(Q_e - Q_t)$  and  $t/Q_t$  versus time  $t$ , in pseudo-first-order and pseudo-second-order kinetic models, respectively, demonstrates the applicability of these models for adsorption of sorbate (MB dye here) on adsorbent (hydrogel samples). The rate constants were calculated from the slope of the straight lines in Figure 5 and Figure 6. The calculated kinetic constants values and the corresponding linear regression correlation constants were given in Table 3. As it can be seen from Table 3, the adsorption process was controlled by pseudo second-order equation in both hydrogel samples, as the correlation coefficient for the first-order equation is lower than that of the second-order equation. In addition, the experimental adsorption capacity values were very close to the model-calculated adsorption capacity data.

**Effect of Initial Concentration of MB**

To investigate the effect of initial concentration of MB on the removal efficiency of MB by hydrogel samples, 0.2 g of hydrogel samples were contacted for 24 h with 100 ml of MB solutions with different initial concentrations (10 to 200 ppm). As shown in Figure 7 the removal efficiency decreased by increasing the initial concentration of dye solution which may be due to the saturation of adsorption sites on the hydrogel samples. At low concentration of dye, there will be unoccupied active sites on the adsorbent surface, and by increasing the initial dye concentration increases, the active sites required for adsorption of the MB dye molecules will decrease. However, with increasing initial concentration of dye, adsorption capacity increases.

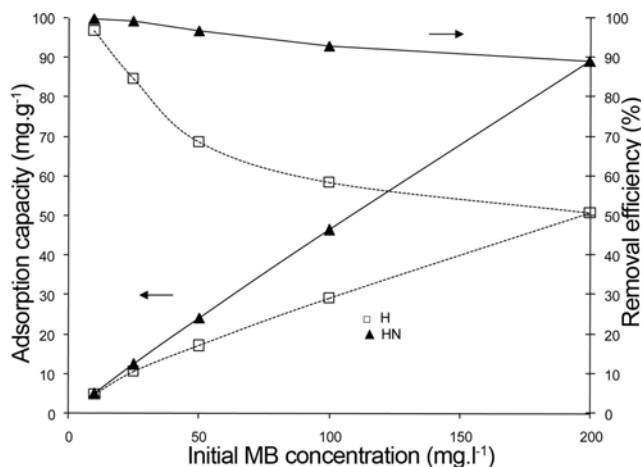


**Figure 7.** The effect of initial concentration of MB on the removal efficiency and adsorption capacity of MB.

**Table 3.** Parameters of pseudo first and second-order reaction kinetics for the adsorption of MB

Adsorbent sample	$Q_e$ (exp)	Pseudo-first-order equation			Pseudo-second-order equation		
		$R^2$	$Q_e$ (cal)	$k_{1,ads}$	$R^2$	$Q_e$ (cal)	$k_{2,ads}$
H	10.59	0.98	10.18	0.0062	0.990	11.17	0.0011
HN	12.43	0.88	8.67	0.0062	0.994	12.85	0.0016

This may be due to the high driving force for mass at a high initial MB concentration. In other words, the residual concentration of MB molecules will be higher for higher initial MB concentrations. In the case of lower concentrations, the ratio of initial number of MB molecules to the available adsorption sites is low and subsequently the fractional adsorption becomes independent of initial concentration [41]. As can be seen from this figure, removal efficiency and adsorption capacity for hydrogel nanocomposite is slightly higher than hydrogel without zeolite. Therefore, the obtained results indicated that zeolite nanoclay incorporation into the hydrogel structure increased not only the swelling capacity of hydrogel but also the adsorption capacity of methylene blue.

**Adsorption Isotherms**

In order to interpret the adsorption process and interactions between adsorbate molecules and adsorbent surface, it was required to use the adsorption isotherms. The adsorption isotherms describe the distribution of adsorbate molecules between the liquid and the solid phases when the adsorption process reaches an equilibrium state. The adsorption isotherms of MB were simulated by using well-known models of Langmuir and Freundlich. The Langmuir model as presented in equation (6) assumes that the removal of MB dye occurs on a homogenous surface by monolayer sorption [42].

$$\frac{C_e}{Q_e} = \left(\frac{1}{Q_{max}}\right)C_e + \frac{1}{Q_{max}b} \tag{6}$$

where  $C_e$  ( $mg \cdot l^{-1}$ ) is the equilibrium MB dye concentration,  $Q_e$  ( $mg \cdot g^{-1}$ ) is the amount adsorbed at equilibrium,  $Q_{max}$  ( $mg \cdot g^{-1}$ ) is the monolayer sorption capacity and  $b$  ( $l \cdot mg^{-1}$ ) is the Langmuir constant.

In contrast, the Freundlich model (equation (7)) is used for the heterogeneous systems which active sites are distributed exponentially. It was assumed that the stronger binding sites are initially occupied, with the binding strength decreasing with increasing degree of site occupation.

$$\log Q_e = \frac{1}{n} \log C_e + \log K_f \tag{7}$$

where  $K_f$  ( $mg \cdot g^{-1}$ ) and  $n$  are the Freundlich constants related to adsorption capacity and adsorption intensity of adsorbents, and can be calculated from the intercept and slope of plot between  $\log Q_e$  and  $\log C_e$ , respectively. The magnitude of the  $n$  gives an indication of favorability of adsorption. The values of  $n$  ranges from 2-10 indicating good adsorption capacity, between 1 to 2 moderate adsorption capacity and

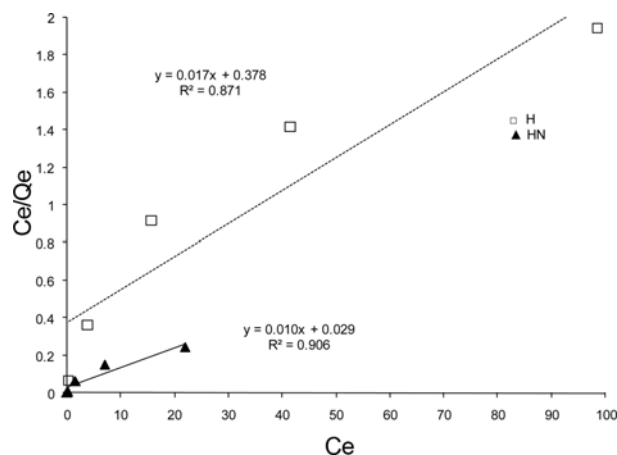


**Figure 8.** Linearized form of Langmuir isotherm for MB adsorption using hydrogel samples.

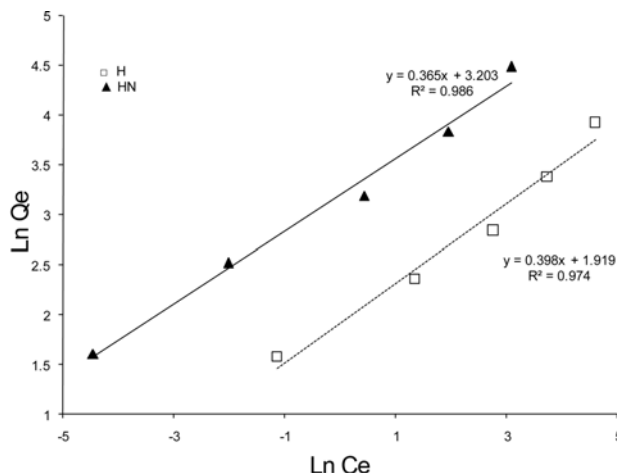


**Figure 9.** Linearized form of Freundlich isotherm for MB adsorption using hydrogel samples.

less than one indicates poor adsorption capacity [43]. The obtained experimental data were fitted with the linearized form of Langmuir and Freundlich models, which was shown in Figure 8 and Figure 9, respectively. The corresponding correlation coefficients and the isotherm constants were calculated and presented in Table 4. From the result obtained, it can be deduced that for both hydrogel samples, the Freundlich isotherm gave a better fit to the experimental data than the Langmuir isotherm owing to the higher  $R^2$  values obtained in the former, suggesting higher probability of

**Table 4.** Parameters of Langmuir and Freundlich equations for the adsorption of MB

Adsorbent sample	$Q_e$ (exp)	Langmuir equation parameter			Freundlich equation parameter		
		$R^2$	$Q_{max}$ (mg/g)	$b$	$R^2$	$n$	$k_F$
H	50.73	0.871	56.81	0.046	0.974	2.51	6.82
HN	89.08	0.906	94.34	0.356	0.986	2.73	24.62

multilayer adsorption over monolayer adsorption in both hydrogel samples [34]. This suggests that some heterogeneity in the surface or pores of hydrogel samples will play a role in dye adsorption. The value of  $n$ , which is above one and lies between 2 to 10, is indicative of favorable adsorption of MB by both hydrogel samples under the experimental conditions. Moreover, the hydrogel nanocomposite adsorbent presented higher  $K_f$  ( $24.62 \text{ mg} \cdot \text{g}^{-1}$ ) for methylene blue than the hydrogel sample without clinoptilolite ( $6.82 \text{ mg} \cdot \text{g}^{-1}$ ). The  $K_f$ -value can be correlated with the variation of surface area of the adsorbent [4]. Higher surface area of hydrogel nanocomposite will generally result in higher adsorption capacity [44]. Also, calculated  $Q_{\text{max}}$  from linearized Langmuir isotherm in the case of hydrogel ( $56.81 \text{ mg} \cdot \text{g}^{-1}$ ) and hydrogel nanocomposite ( $94.34 \text{ mg} \cdot \text{g}^{-1}$ ) are close to experimental amount of  $Q$  ( $50.73$  and  $89.08 \text{ mg} \cdot \text{g}^{-1}$ , respectively).

### Mechanism of Adsorption

To study the adsorption of MB on H and HN, hydrogel samples were placed in aqueous solution of MB and then allowed to reach equilibrium for 24 h. As shown in Figure 10, the adsorption mechanism can be followed from the change of color of hydrogel samples before and after putting in MB solution. As it was seen, the prepared hydrogel samples became bluish compared with the original color of hydrogel samples and at the same time hydrogel samples showed high degree of swelling due to the adsorption of MB. The adsorption mechanism of MB by hydrogel nanocomposite is schematically shown in Figure 11. The

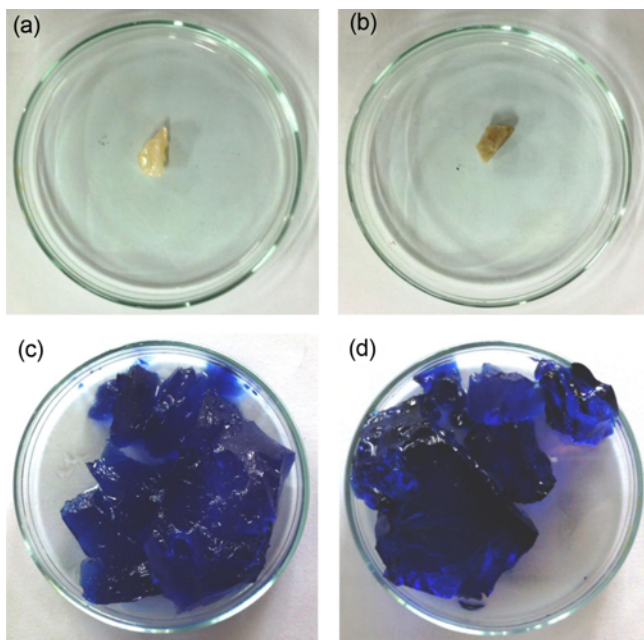


**Figure 10.** Photographs of hydrogel and hydrogel nanocomposite samples before (a, b) and after immersion in MB dye solution (c, d).

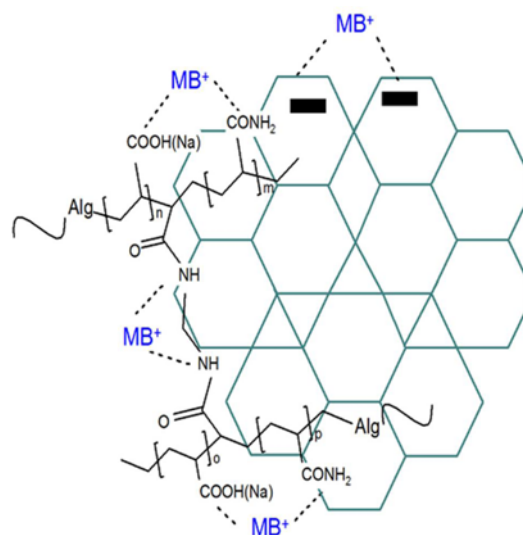


**Figure 11.** Schematic illustration of adsorption of cationic MB dyes on to the prepared hydrogel samples.

hydrogel nanocomposite was prepared by graft copolymerization of acrylic acid and acrylamide onto sodium alginate in the presence of MBA as crosslinking agent and clinoptilolite zeolite. It is known that basic dyes or cationic dyes like MB upon dissolution release colored dye cations into the solution. As one can easily see, the hydrogel samples adsorbed MB dye through swelling and penetration of dye to hydrogel network due to the electrostatic forces between imine groups of cationic methylene blue and anionic structure of hydrogel samples composed of carboxylic and amide groups. This event was confirmed by shifts in FT-IR spectra of functional groups of hydrogel as a result of adsorption of MB. Also, negative surface charge of natural clinoptilolite zeolite can serve to adsorb cationic MB dye molecules via electrostatic attraction. Therefore, it can be concluded that the type of interaction in this case can be described by chelation and ion exchange. As shown in previous section about adsorption isotherms, hydrogel nanocomposite has higher adsorption capacity in comparison with hydrogel sample without clinoptilolite as adsorbent. High adsorption capacity indicates strong electrostatic force of attraction between dye molecules and sorbent binding sites as a result of addition of clinoptilolite [44].

### Desorption and Reusability Studies

For practical applications, desorption experiments were performed to regenerate dye loaded hydrogels and use it in the adsorption and desorption processes to examine the reusability potential of hydrogels for economical purposes. Table 5 showed the removal efficiency and desorption ratio of MB dye in five cycles. As shown in Table 5, the removal efficiency showed a little decrease for both hydrogel as a result of occupation of some adsorption sites by MB dye.

**Table 5.** Removal efficiency and desorption ratio behaviors of MB onto hydrogel samples

Cycle	H		HN	
	Removal efficiency	Desorption ratio	Removal efficiency	Desorption ratio
1	84.72	84.32	99.47	98.68
2	79.65	79.92	98.34	97.52
3	73.39	79.08	97.65	96.56
4	68.58	78.2	97.15	95.48
5	67.95	77.52	96.59	95.16

This means that the adsorption in the next runs occurred only on the adsorption sites which were created due to the desorption of MB dye from the surface and pores of the hydrogel samples. Incomplete desorption could be attributed to the formation of very strong complexes between the functional groups of the adsorbents (like NH<sub>2</sub>, OH) and MB. Although the removal efficiency and desorption ratio decreased per cycle in both hydrogel samples, in the fifth cycle the hydrogel nanocomposite could remove about 96.59 % of MB. In comparison the removal efficiency of hydrogel sample with out clinoptilolite is about 77.52 %, meaning the excellent reusability of hydrogel nanocomposite samples.

### Conclusion

The synthesis of NaAlg-g-p(AA-co-AAm)/Clin hydrogel nanocomposite was performed by free radical polymerization method. The application of prepared hydrogel nanocomposite was investigated as an adsorbent for the removal of MB dye from aqueous solutions. It was found that the removal efficiency of MB using this hydrogel nanocomposite as an adsorbent was about 99.47 % in comparison with 84.72 % in the case of hydrogel without zeolite. The obtained results indicated that zeolite incorporation into the hydrogel structure increased not only the swelling capacity but also the adsorption capacity of methylene blue. The batch sorption kinetics was tested and the pseudo second-order kinetic model was fitted well with experimental results. The equilibrium data from experiments were analyzed by the Langmuir and Freundlich models that showed better fit with Freundlich model and multilayer adsorption. Desorption studies showed that after 5 cycles; hydrogel nanocomposite samples had a good adsorption behavior for MB dye. Studies showed that swelling and penetration of dye to hydrogel network due to the electrostatic forces between hydrogel samples and MB dye were the governing adsorption mechanism.

### Acknowledgements

The financial support of this work by University of Tabriz is gratefully acknowledged.

### References

1. C. Fernández, M. S. Larrechi, and M. P. Callao, *Trac-Trends Anal. Chem.*, **29**, 1202 (2010).
2. M. A. Mohd Salleh, D. Kh. Mahmoud, W. A. W. Abdul Karim, and A. Idris, *Desalination*, **280**, 1 (2011).
3. Q. Li, Q. Y. Yue, H. J. Sun, Y. Su, and B. Y. Gao, *J. Environ. Manage.*, **91**, 1601 (2010).
4. D. A. Fungaro, L. C. Grosche, A. S. Pinheiro, J. C. Izidoro, and S. I. Borrelly, *Orbital: Electron. J. Chem.*, **2**, 235 (2010).
5. A. A. Kale, A. S. Burungale, M. R. Bhandare, and R. V. Kashalkar, *J. Chem. Pharm. Res.*, **4**, 772 (2012).
6. Y. M. Slokar and A. M. L. Marechal, *Dyes Pigment.*, **37**, 335 (1998).
7. P. Cooper, *J. Soc. Dyers. Colour.*, **109**, 97 (1993).
8. K. Gupta and Suhas, *J. Environ. Manage.*, **90**, 2313 (2009).
9. H. Kasgoz and A. Durmus, *Polym. Adv. Technol.*, **19**, 838 (2008).
10. Y. Al-Degs, M. A. M. Khraisheh, S. J. Allen, and M. N. A. Ahmad, *Sep. Sci. Technol.*, **36**, 91 (2011).
11. C. A. P. Almeida, N. A. Debacher, A. J. Downs, L. Cottet, and C. A. D. Mello, *J. Colloid Interface Sci.*, **332**, 46 (2009).
12. M. M. Nassar and M. S. Elgeundi, *J. Chem. Technol. Biotechnol.*, **50**, 257 (1991).
13. W. Shaobin and P. Yuelian, *Chem. Eng. J.*, **156**, 11 (2010).
14. O. Hamdaoui, *J. Hazard. Mater.*, **135**, 264 (2006).
15. A. Ahmad, M. Rafatullah, O. Sulaiman, M. H. Ibrahim, and R. Hashim, *J. Hazard. Mater.*, **170**, 357 (2009).
16. G. Annadurai, R. Juang, and D. Lee, *J. Hazard. Mater.*, **92**, 263 (2002).
17. M. Kaplan and H. Kasgoz, *Polym. Bull.*, **67**, 1153 (2011).
18. H. A. Abd El-Rehim, E. A. Hegazy, and D. A. Diaa, *React. Funct. Polym.*, **72**, 823 (2012).
19. N. Seetapan, J. Wongsawaeng, and S. Kiatkamjornwong, *Polym. Adv. Technol.*, **22**, 1685 (2011).
20. S. Kundakci, O. B. Uzum, and E. Karadag, *React. Funct. Polym.*, **68**, 458 (2008).
21. G. Bagheri Marandi, G. R. Mahdavinia, and S. Ghafary, *J. Polym. Res.*, **18**, 1487 (2011).
22. B. Armagan, O. Ozdemir, M. Turan, and M. S. Celik, *J. Chem. Technol. Biotechnol.*, **78**, 725 (2003).
23. B. Armagan, M. Turan, and M. S. Celik, *Desalination*, **170**, 33 (2004).
24. A. S. Sheta, A. M. Falatah, M. S. Al-Sewailem, E. M. Khaled, and A. S. H. Sallam, *Microporous Mesoporous Mat.*, **61**, 127 (2003).
25. P. Schexnailder and G. Schmidt, *Colloid. Polym. Sci.*, **287**, 1 (2009).
26. T. Singh and R. Singhal, *J. Appl. Polym. Sci.*, **125**, 1267 (2012).
27. B. Ozkahraman, I. Acar, and S. Emik, *Clean-Soil, Air, Water*, **39**, 658 (2011).



28. G. Guclu, E. Al, S. Emik, T. B. Iyim, S. Ozgumus, and M. Ozyurek, *Polym. Bull.*, **65**, 333 (2010).
29. S. Zhao, F. Zhou, L. Li, M. Cao, D. Zuo, and H. Liu, *Compos. Pt. B-Eng.*, **43**, 1570 (2012).
30. A. Ely, M. Baudu, M. Ould Sid, A. Ould Kankoub, and J.-P. Basly, *Chem. Eng. J.*, **178**, 168 (2011).
31. N. M. Mahmoodi, B. Hayati, and M. Arami, *Ind. Crop. Prod.*, **35**, 295 (2012).
32. A. Pourjavadi, H. Ghasemzadeh, and R. Soleyman, *J. Appl. Polym. Sci.*, **105**, 2631 (2007).
33. S. Hua and A. Wang, *Carbohydr. Polym.*, **75**, 79 (2009).
34. R. P. Dumitriu, G. R. Mitchell, and C. Vasile, *Polym. Int.*, **60**, 222 (2011).
35. D. E. Owens III, Y. Jian, J. E. Fang, B. V. Slaughter, Y.-H. Chen, and N. A. Peppas, *Macromolecules*, **40**, 7306 (2007).
36. M. A. Moharram, L. S. Balloomal, and H. M. El Gendy, *J. Appl. Polym. Sci.*, **59**, 987 (1996).
37. M. Zendehtel, A. Barati, and H. Alikhani, *Polym. Bull.*, **67**, 343 (2011).
38. D. Baybas and U. Ulusoy, *J. Hazard. Mater.*, **187**, 241 (2011).
39. S. Lagergren, Zur theorie der sogenannten adsorption gelöster stoffe, Kungliga Svenska Vetenskapsakademiens Handlingar, **24**, 1 (1898).
40. Y. S. Ho and G. McKay, *Process Biochem.*, **34**, 451 (1999).
41. S. A. Umoren, U. J. Etim, and A. U. Israel, *J. Mater. Environ. Sci.*, **4**, 75 (2013).
42. N. A. Oztas, A. Karabakana, and O. Topala, *Microporous Mesoporous Mat.*, **111**, 200 (2008).
43. O. Hamdaouia and E. Naffrechoux, *J. Hazard. Mater.*, **147**, 381 (2007).
44. R. Ansari and Z. Mosayebzadeh, *Chem. Pap.*, **65**, 1 (2011).